An analysis of the 2023 summer and fall marine heat waves on the Newfoundland and Labrador Shelf

Nancy Soontiens[1], Heather J. Andres[1], Jonathan Coyne[1], Frédéric Cyr[1,*], Peter S. Galbraith[2], Jared Penney[1]

[1]Northwest Atlantic Fisheries Centre, Fisheries and Oceans Canada, St. John's, NL, A1C 5X1, Canada
[2]Institut Maurice-Lamontagne, Fisheries and Oceans Canada, Mont-Joli, QC, G5H 3Z4, Canada
[*]Now at: Center for Fisheries and Ecosystem Research, Fisheries and Marine Institute of Memorial University of Newfoundland, St. John's, NL

Correspondence to: Nancy Soontiens (nancy.soontiens@dfo-mpo.gc.ca)

Abstract

In this study, we investigated a series of moderate to severe surface marine heat waves (MHWs) impacting the Newfoundland and Labrador Shelf during the summer and fall of 2023. Using a combination of ocean model reanalysis data, in situ data collected under the Atlantic Zone Monitoring Program (AZMP), and atmospheric reanalysis data, we explored several factors that contributed to the intensity of these MHWs. We concluded that first, due to an unusually cold spring and abnormally fresh conditions advected from upstream, the water column was highly stratified. Second, atmospheric conditions were calm, anomalously warm, and wind speeds were unusually low for prolonged periods in the summer. The combination of increased stratification and lower wind speeds caused a reduction in vertical mixing, limiting the exchange of warm surface waters with colder waters below and amplifying the retention of heat near the surface. However, by the late fall, the signature of the surface heat wave had vanished when the cooler subsurface waters were mixed vertically due to increased winds, storms, and surface cooling. During the most intense MHW in July 2023, we found that this event was confined to the surface as demonstrated by temperature anomalies along several standard transects which showed a thin layer of warm anomalies in the upper 10 m and cold anomalies below. Consequently, the vertical extent and distribution of MHWs are important considerations when exploring ecosystem impacts because not all elements of the ecosystem are equally sensitive to surface conditions. Finally, these results suggest that ocean model nowcast and reanalysis products can complement observational methods for studying MHWs in near-real time over large geographic areas and at multiple depths.

31 **1 Introduction**

32 In the summer of 2023, the North Atlantic Ocean experienced a series of significant marine heat waves (MHWs) sparking

33 media attention and public interest in the associated record-setting high ocean temperatures. These MHWs were first detected

34 in the Northeast Atlantic in June and, later, in the Northwest Atlantic in July (Copernicus, 2023). Ocean warming and MHWs

35 can have significant impacts on the marine ecosystem (e.g., LeGrix et al., 2021; Geoffroy et al., 2023, Smith et al., 2023), air-

36 sea exchange (e.g. Edwing et al., 2024) and weather (e.g., Frölicher et al., 2018). Globally, MHWs are occurring more

37 frequently and with greater duration (Oliver et al, 2018; IPCC, 2019; IPCC, 2023). As such, it is critical to develop a more

38 complete understanding of their drivers (Oliver et al., 2021) which will lead to improved real-time monitoring efforts and

39 forecasting capabilities (e.g., McAdam et al., 2023).

40

41 Studies of MHWs in the Northwest Atlantic have documented the role of air-sea fluxes and oceanic processes like advection

42 in the onset and decay of MHWs. Schlegel et al. (2021) applied statistical methods to a combination of remotely-sensed sea

43 surface temperature data and atmospheric and oceanic reanalyses to link latent heat flux and mixed layer depth as drivers of

44 MHWs over the Northwest Atlantic continental shelf. They show that the onset of many surface MHWs in this area is linked

45 with a positive air-sea heat flux anomaly into the ocean, most often driven by latent heat flux and shortwave radiation, but that

46 the decay is more often associated with oceanic processes like advection and mixing. Other studies have correlated MHWs

47 with large-scale atmospheric conditions and spatial variability in heat flux anomalies. For example, Perez et al. (2021) link the

48 2015/16 MHW in the Northwest Atlantic to the position of the jet stream modifying the spatial distribution of heat fluxes, a

49 finding confirmed by Sims et al. (2022), who further correlate sea surface temperature (SST) and sea surface salinity anomalies

50 near the shelf break in a subregion (48–70° W, 40–48° N) with the North Atlantic Oscillation (NAO). These studies indicate

51 that a combination of oceanic and atmospheric processes drove the 2015/16 MHW. Other studies link abrupt sea ice melt and

52 strong stratification with intensified surface MHWs in the Arctic (see e.g. Barkhordarian et al., 2024; Richaud et al., 2024) and

53 recent work by Sun et al. (2024) identifies a strong relationship between mixed layer depth shoaling, restratification, and MHW

54 occurrence globally.

55

56 In this study, we describe a series of MHWs that occurred on the Newfoundland and Labrador (NL) Shelf during the summer

57 and fall of 2023. The NL Shelf is a region of economic, environmental, and cultural importance as it supports numerous

commercial, recreational, and Indigenous fisheries (Templeman, 2010). The oceanographic conditions are characteristic of Arctic and subarctic environments, and are influenced by the Labrador Current, which transports relatively cold and fresh water equatorward along the continental shelf (e.g., Lazier and Wright, 1993; Fratantoni and Pickart, 2007). The region undergoes interannual variability cycling through warm and cold phases associated with changes in air temperature, sea ice conditions, and climate indices such as the NAO (Petrie, 2007; Urrego-Blanco and Sheng, 2012; Han et al., 2019; Cyr and Galbraith, 2021). These warm and cold phases are linked to marine ecosystem characteristics such as the timing of the spring phytoplankton bloom and primary and secondary productivity (Cyr et al., 2024a), as well as the productivity of higher trophic levels (Cyr et al., 2024b). Variability in the offshore transport of the Labrador Current (e.g., Jutras et al., 2023) is also linked with ecosystem characteristics such as marine bivalve growth as suggested by Poitevin et al. (2019). Seasonal ice cover in the region has important implications for stratification, and in turn, primary productivity (e.g., Wu et al., 2007).

We conduct our analysis over several geographic subregions of the NL Shelf with distinct ecosystem characteristics, as described in Section 2.2 and explore the influence of several meteorological and oceanographic phenomena such as winds, air-sea heat fluxes, stratification, and advection on this series of MHWs. Studying the factors driving MHWs on the NL Shelf will support understanding in how these events may impact the local marine ecosystem.

2 Methods

2.1 Datasets

A number of datasets were used in this study. MHWs were characterised using the sea surface temperature (SST) from product ref. no. 1 (Table 1) which is a 1/12 degree global ocean reanalysis (herein GLORYS12V1) covering December 31, 1992 to December 25, 2023. Daily mean temperature and salinity fields were also used to describe oceanographic conditions such as stratification, depth-averaged temperature, and freshwater density. Sea ice concentration was also analysed to characterise the monthly maximum sea ice extent, defined as regions where the concentration is greater than 0.15. Sea ice volume, defined as the product between the GLORYS12V1 sea ice concentration, sea ice thickness, and grid cell area, summed over the NL Shelf was also calculated and analysed. Following recommendations by McDougall et al. (2021), we interpreted the GLORYS12V1 prognostic temperature and salinity variables to be conservative temperature and preformed salinity – a salinity variable not affected by biogeochemistry – scaled by a factor of $u_{ps} = \frac{35.16504}{35}$g kg^{-1}. Finally, the mixed layer depth, provided as a GLORYS12V1 output and defined as the depth where the density increase compared to density at 10 m depth corresponds to a temperature decrease of 0.2°C in local surface conditions, was also considered.

The GLORYS12V1 dataset was complemented by temperature and salinity profiles from product ref. no. 2 (CASTS; Table 1) which is composed of historical profiles in Atlantic Canada and the Eastern Arctic dating back to 1912, but here limited to the

period 1993-2023. Many of the CASTS profiles used in this study were collected under the Atlantic Zone Monitoring Program (AZMP; Therriault et al., 1998) which routinely monitors core stations and transects at annual and seasonal frequencies. Two AZMP transects (Seal Island and Flemish Cap) and one high-frequency sampling station (Station 27) were considered in this study (Fig. 1). To facilitate comparison with GLORYS12V1, the CASTS potential temperature and practical salinity variables were converted to conservative temperature and preformed salinity using the Python implementation of the Gibbs-Seawater (GSW) Oceanographic Toolbox (McDougall and Barker, 2011).

Finally, 10-metre wind speeds were taken from product ref. no. 3 which is a global atmospheric reanalysis (ERA5; Table 1). Daily mean wind speeds were smoothed using an 11-day rolling mean in order to isolate synoptic-scale events by removing high-frequency variability. Additionally, the role of air-sea interaction was examined using the following ERA5 variables: net surface short-wave radiation (Q_{swr}), net surface long-wave radiation (Q_{lwr}), surface latent heat flux (Q_{lh}), and surface sensible heat flux (Q_{sh}). Following Denexa et al. (2024), the sum of these four components was used to determine the net surface heat flux (Q) and Q_{swr} was taken as the surface value. All heat flux and radiation variables are positive downwards and represent a daily average. The ERA5 daily averaged 2-metre air temperature was also analysed. Climatologies for all ERA5 variables were calculated in the same way as the MHW climatologies. Bathymetry data for plotting is taken from product ref. no. 4 (ETOPO 2022; Table 1).

Product Ref. No.	Product ID & type	Data Access	Documentation
1	GLOBAL_MULTIYEAR_PHY_001_030 (GLORYS12V1), numerical models	EU Copernicus Marine Service Product (2023)	Product User Manual (PUM): Drévillon et al., 2023a Quality Information Document (QUID): Drévillon et al., 2023b Journal article: Lellouche et al., 2021
2	CASTS, observed temperature and salinity profiles	Federated Research Data Repository, https://doi.org/10.20383/102.0739	Coyne et al., 2023
3	ERA5, atmospheric reanalyses	Copernicus Climate Change Service (2023)	Product reference: Hersbach et al., 2023 Journal article: Hersbach et al., 2020
4	ETOPO 2022, gridded bathymetry	https://doi.org/10.25921/fd45-gt74	Product reference: NOAA National Centers for Environmental Information, 2022

105 **Table 1: Overview of the data products used in this study.**

106 **2.2 Marine heat wave definitions**

107 Following Hobday et al. (2016), we defined a MHW as a period of 5 days or longer during which the daily averaged SST

108 exceeds the climatological 90th percentile (T_{90}) for the given time of year. The World Meteorological Organization

109 recommends, when possible, to use a 30-year time series (1991-2020) to calculate climatologies (World Meteorological

110 Organization, 2017). In this study, because GLORYS12V1 starts in 1993, the climatology was calculated for each day of the

111 year over 1993 to 2022. See the Supplementary Materials for the temperature and freshwater density trends over this period

112 (Fig. S1) and a discussion on the sensitivity of the results to the climatological period. The climatological mean and 90th and

113 10th percentiles were determined using an 11-day window (see Hobday et al. (2016) for details) and the percentiles and

114 climatological mean were smoothed using a 31-day rolling average.

115

116 Spatially, the analysis was performed over 1) every grid cell in GLORYS12V1 from 65° W to 39° W and 41° N to 62° N and

117 2) the spatially averaged SST in regions relevant to the NL Shelf ecosystem. Shown in Fig. 1 (a), these regions are the Labrador

118 Shelf (LS), the Northeast Newfoundland Shelf (NNS), the Grand Banks (GB), and Flemish Cap (FC). Each represents an area

119 of distinct primary productivity and a well-defined food web system (Open Government, 2014; Pepin et al., 2014). A fifth

120 region covering the entire NL Shelf (Fig. 1 (c)) was also included.

121

122 Finally, using Δ as the difference between T_{90} and the climatological mean, we followed Hobday et al. (2018) to define four

123 heat wave categories when temperature T exceeds T_{90} as follows: moderate ($T_{90} \leq T < T_{90} + \Delta$), strong ($T_{90} + \Delta \leq T <$

124 $T_{90} + 2\Delta$), severe ($T_{90} + 2\Delta \leq T < T_{90} + 3\Delta$), and extreme ($T \geq T_{90} + 3\Delta$). Some additional MHW metrics, including the

125 start and end dates (t_s and t_e), duration or number of MHW days (D), and mean, maximum, and cumulative intensities (i_{mean},

126 i_{max}, i_{cum}, respectively), suggested by Hobday et al. (2016) are reported in Table 2. The mean intensity is the mean of the

127 temperature anomaly, the maximum intensity is the maximum of the temperature anomaly, and the cumulative intensity is the

128 integrated daily temperature anomaly over the MHW period.

129 **2.3 Stratification, depth-averaged temperature, and freshwater density**

130 The 2023 daily time series and climatologies (1993-2022) of three additional metrics (stratification, depth-averaged

131 temperature, and freshwater density) were calculated. The metric climatologies were determined using the same methodology

132 as applied to the SST climatologies. First, the stratification was assessed by calculating the squared-buoyancy

133 frequency, $N^2(z)$, over the entire water column using the GSW Oceanographic Toolbox (McDougall and Barker, 2011) and

134 then, its vertical maximum, N^2_{max}, was used as a measure of stratification. A large value indicates strong stratification which

135 can limit the vertical exchange of heat and salt content. This quantity was analysed as a spatial average over each region and

136 at the grid cell closest to Station 27 where comparisons with observed data were made. In order to compare modelled and

137   observed profiles of $N^2(z)$ at Station 27, the observed temperature and salinity fields were first interpolated to GLORYS12V1

138   depth levels, then $N^2(z)$ was calculated, and then its vertical maximum was determined. Furthermore, we defined the mixed

139   layer depth as the depth of the vertical maximum of $N^2(z)$.

140

141   Second, the depth-averaged temperature and freshwater density were used to examine the daily time evolution of temperature

142   and freshwater content in the uppermost 20 m spatially averaged over the NL Shelf region (see Supplementary Material Fig.

143   S5 for additional depth bins). The depth-averaged temperature is defined as

144    $$T_{z_1-z_2} = \frac{\int_{z_1}^{z_2} T\,dz}{\int_{z_1}^{z_2} dz},$$

145   where T is the temperature, z_1 and z_2 are the depth levels over which the integral is calculated. The freshwater density is

146    $$FWD_{z_1-z_2} = \frac{\int_{z_1}^{z_2} \frac{\rho(T,S,p)}{\rho(T,0,p)}\frac{S_{ref}-S}{S_{ref}}\,dz}{\int_{z_1}^{z_2} dz} \frac{\int_{z_1}^{z_2} \frac{\rho(T,S,p)}{\rho(T,0,p)}\frac{S_{ref}-S}{S_{ref}}\,dz}{\int_{z_1}^{z_2} dz},$$

147   where $\rho(T,S,p)$ is the in situ density calculated with the GSW Oceanographic Toolbox, S is the salinity, p is the pressure,

148    $\rho(T,0,p)$ is the density of seawater with zero salinity, and S_{ref} is a reference salinity of 35 g kg^{-1}. Quantities that were spatially

149   averaged over a region or across a transect are denoted by an overbar symbol. For example, the spatially averaged sea surface

150   temperature over a region is defined by

151    $$\overline{SST} = \frac{\int_{area} SST\,dA}{\int_{area} dA}.$$

152   **3 Results**

153   From July through October, MHWs were detected over most of the Northwest Atlantic (Fig. 1). Over the NL Shelf, MHW

154   categories mainly ranged from moderate to severe with spatial variability in the intensity and duration. No MHWs were present

155   continuously throughout the entire July to October period, but rather a series of MHWs transpired in each region (Table 2).

156   Each MHW period was associated with higher-than-typical stratification, in many cases exceeding the 90th percentile. The

157   most intense and longest duration MHW began in July in FC. Each of the other subregions experienced their strongest MHW

158   (in terms of maximum and mean intensity) around the same time, also commencing in July. A large portion of the southern

159   GB received relatively short duration and low intensity MHWs while both LS and NNS contained localised areas of higher

160   intensity MHWs (e.g., up to severe) that were approximately collocated with areas of greater total MHW days in the July

161   through October period (Fig. 1).

162
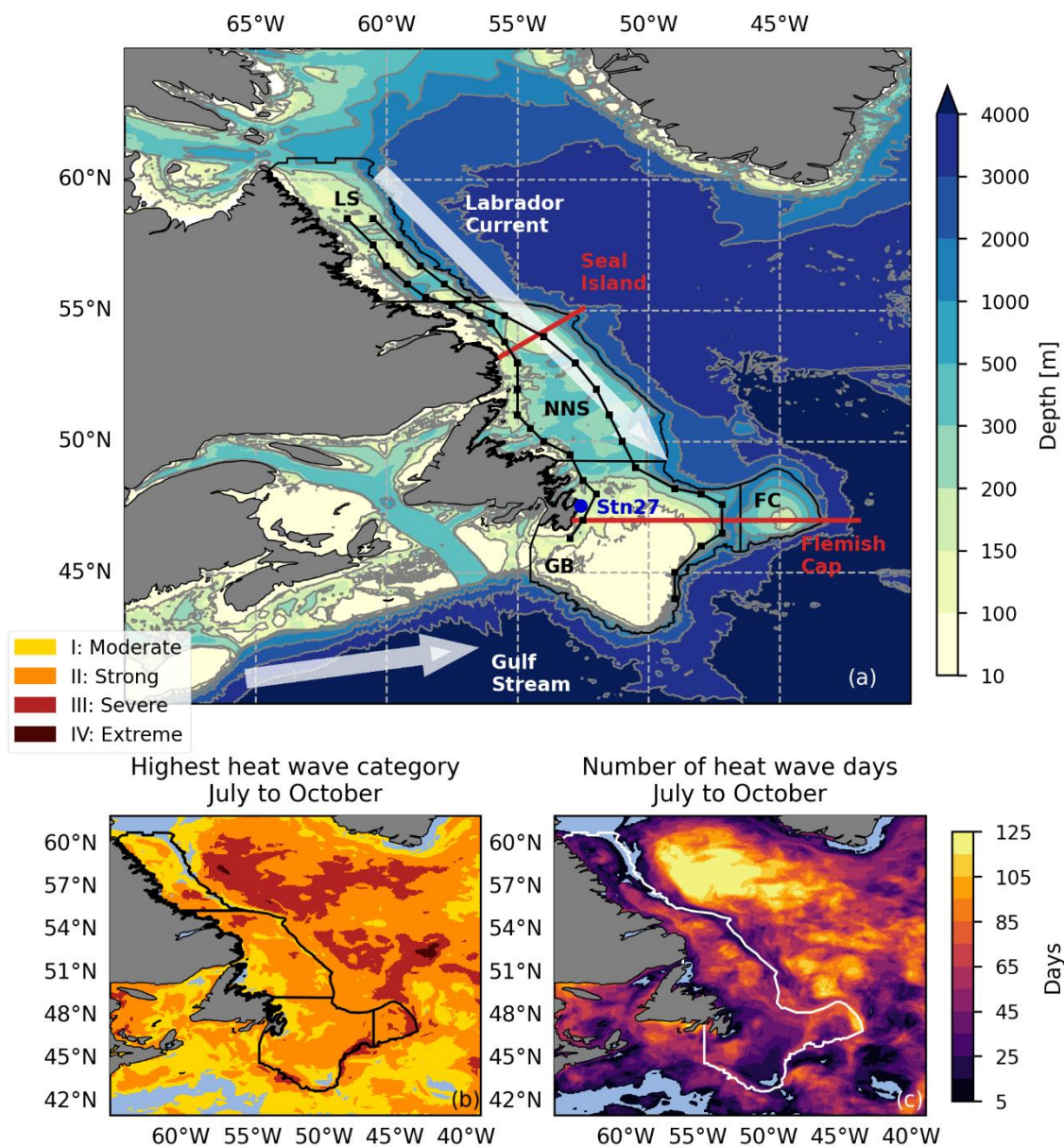
Figure 1: (a) Bathymetry from ETOPO 2022 (product ref. no. 4) in the study region. The thin black lines represent the regions over which MHW statistics are calculated: Labrador Shelf (LS), Northeast Newfoundland Shelf (NNS), Grand Banks (GB), and Flemish Cap (FC). Standard AZMP transects Seal Island and Flemish Cap are represented by the red lines. The dark blue dot is the location of Station 27 (Stn27). Light colored arrows represent schematics of the Labrador Current and Gulf Stream. Black line segments with dots represent the Outer and Inner Shelf transects. **(b)** Spatial map of highest heat wave categories in July through October 2023 calculated from GLORYS12V1 (product ref. no. 1). Subregion polygons are shown for reference in black. **(c)** Total number of heat wave days July through October 2023 (maximum 122 days), also calculated from the GLORYS12V1 product. The white line represents the polygon used to define the entire NL Shelf. The region definitions are derived from Ecosystem Production Units (Pepin et al., 2014) and contain information licensed under the Open Government Canada Licence - Canada.

174 When the MHW metrics were determined by spatially averaging over the entire NL Shelf, the result was three MHW periods

175 (Table 2). These three periods approximately coincide with the MHW periods identified in the regional analysis. However, the

176 late August MHW in FC and NNS is not captured in the larger spatial average. Nevertheless, we used MHW metrics over the

177 entire NL Shelf region to identify local oceanographic and meteorological conditions that contributed to the evolution of this

178 series of MHWs.

179

Region	t_s Start date	t_e End date	D MHW days	i_{max} (℃)	i_{mean} (℃)	i_{cum} (℃ days)	$<\overline{N^2_{max}}>$ (10⁻⁴ s⁻²)	$<\overline{N^2_{max_{clim}}}>$ (10⁻⁴ s⁻²)	$<\overline{N^2_{max_{90th}}}>$ (10⁻⁴ s⁻²)
Labrador Shelf (LS)	2023-07-16 2023-10-07	2023-07-27 2023-10-23	11 16	2.03 1.01	1.77 0.88	214.50 224.47	12.94 5.50	10.10 4.30	12.70 6.00
Northeast Newfoundland Shelf (NNS)	2023-07-16 2023-08-22 2023-09-14 2023-10-09	2023-08-10 2023-09-01 2023-09-19 2023-10-30	25 10 5 21	3.23 2.32 1.60 1.63	2.53 2.1 1.51 1.26	1579.88 209.94 37.68 553.66	14.48 13.54 10.25 5.61	8.95 9.56 7.34 4.21	10.70 11.52 9.06 5.84
Grand Banks (GB)	2023-07-15 2023-09-07	2023-08-06 2023-09-24	22 17	4.01 3.02	2.92 2.22	1411.51 641.43	12.97 12.17	7.46 9.60	9.07 10.94
Flemish Cap (FC)	2023-07-08 2023-08-27 2023-09-05	2023-08-08 2023-09-01 2023-09-24	31 5 19	5.5 2.11 3.59	3.71 1.89 2.78	3566.89 47.28 1002.69	9.83 9.40 10.51	4.88 7.42 7.80	6.46 9.11 9.35
Entire NL Shelf	2023-07-14 2023-09-06 2023-10-10	2023-08-08 2023-09-23 2023-10-24	25 17 14	2.74 1.76 1.24	2.05 1.37 1.01	1281.54 396.52 198.37	11.75 7.78 5.35	10.11 6.43 4.22	12.65 8.93 5.87

180 **Table 2: MHW metrics and stratification for each region and the entire NL Shelf calculated from GLORYS12V1 (product ref. no.**
181 **1). For MHW metrics, t_s and t_e are the start and end dates of each heat wave, D is the duration or number of MHW days, i_{max}, i_{mean},**
182 **and i_{cum} are the maximum, mean, and cumulative intensities derived from the spatially averaged sea surface temperature anomaly**
183 **during each heat wave period. For stratification, $\overline{N^2_{max}}$, $\overline{N^2_{max_{clim}}}$, and $\overline{N^2_{max_{90th}}}$ are the spatially averaged quantities from 2023, the**
184 **1993-2022 climatological mean, and the 1993-2022 90th percentile, respectively. The angled brackets, < >, denote a time average**
185 **over the MHW period.**

186

187 An intriguing feature of this series of MHWs was that it was pre-conditioned by an unusually cold spring (Fig. 2 (a)-(b)). In

188 mid-June, spatially averaged SST anomalies over the entire shelf were as low as -0.56℃. In some areas, such as the

189 southwestern extent of GB and coastal regions of southern NNS, monthly averaged SST anomalies in June were below -1.50

190 ℃ (Fig. 2 (b)). In contrast, anomalies in July were positive over nearly the entire NL Shelf and the highest anomalies occurred

191 in the FC region. High positive anomalies continued over most of the NL Shelf in August, but the highest anomalies were

192 found in the NNS region. In September, high anomalies returned to the FC area and were concentrated in areas with steep

193 bathymetric gradients that are strongly influenced by the Labrador Current, suggesting a possible advective source of warm

194 water from upstream. Finally, October saw a reduction in the strength of the anomalies, but SSTs were still warmer than usual
195 across the entire NL Shelf.
196
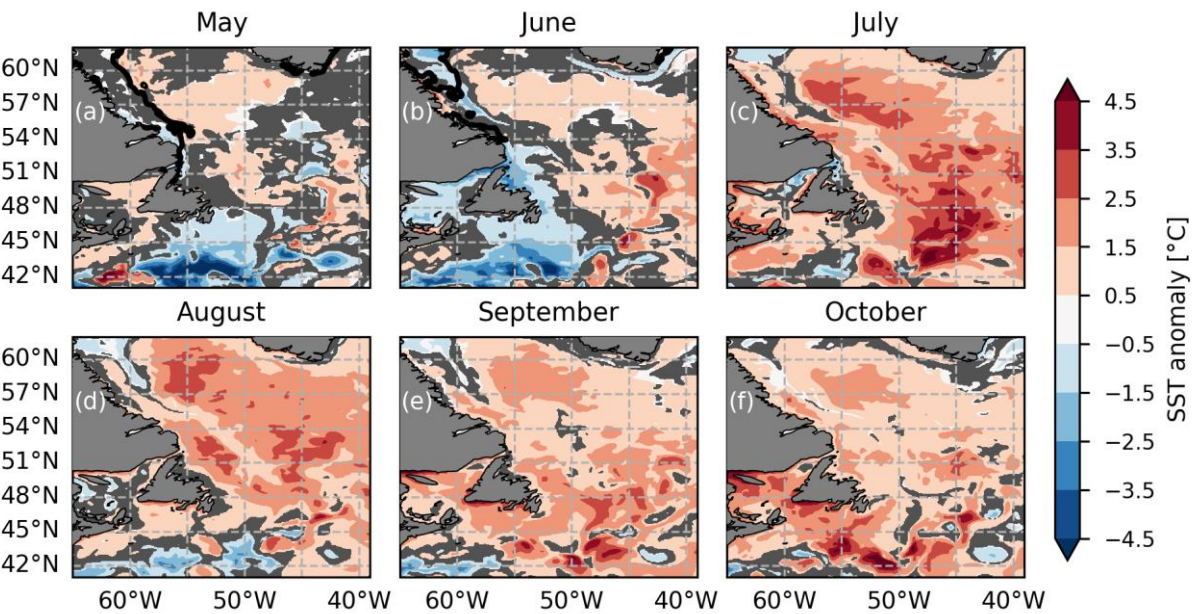
197
198 **Figure 2: Sea surface temperature anomaly from GLORYS12V1 (product ref. no. 1) averaged over (a) May, (b) June, (c) July, (d)**
199 **August, (e) September, and (f) October 2023. A reference period of 1993-2022 is used to calculate climatology. The thick black**
200 **contours in (a) and (b) indicate the monthly maximum sea ice extent from the GLORYS12V1 in 2023. GLORYS12V1 had no sea ice**
201 **in this area from July through October. The grey shading represents regions where the absolute value of the anomaly is less than**
202 **0.5 times the interannual standard deviation of the monthly mean sea surface temperature.**

203

204 In addition to unusually cold spring SSTs (Fig. 2 (a)-(b)), subsurface temperatures from about 10-50 m in July were below
205 normal across the Seal Island and Flemish Cap transects in both GLORYS12V1 (product ref. no. 1) and AZMP (product ref.
206 no. 2) profiles (Fig. 3 (a)-(b)). Both transects displayed a very warm surface layer reaching to approximately 10 m in depth.
207 Additionally, the Seal Island transect showed anomalously fresh conditions in the upper 20 m across most of the transect in
208 July (Fig. 3 (c)), particularly over the shelf break. Along the Flemish Cap transect, fresh signals were not as strong as at Seal
209 Island at this time, but salinity anomalies between -0.25 g kg^{-1} and -0.75 g kg^{-1} were apparent near the coast.
210

212
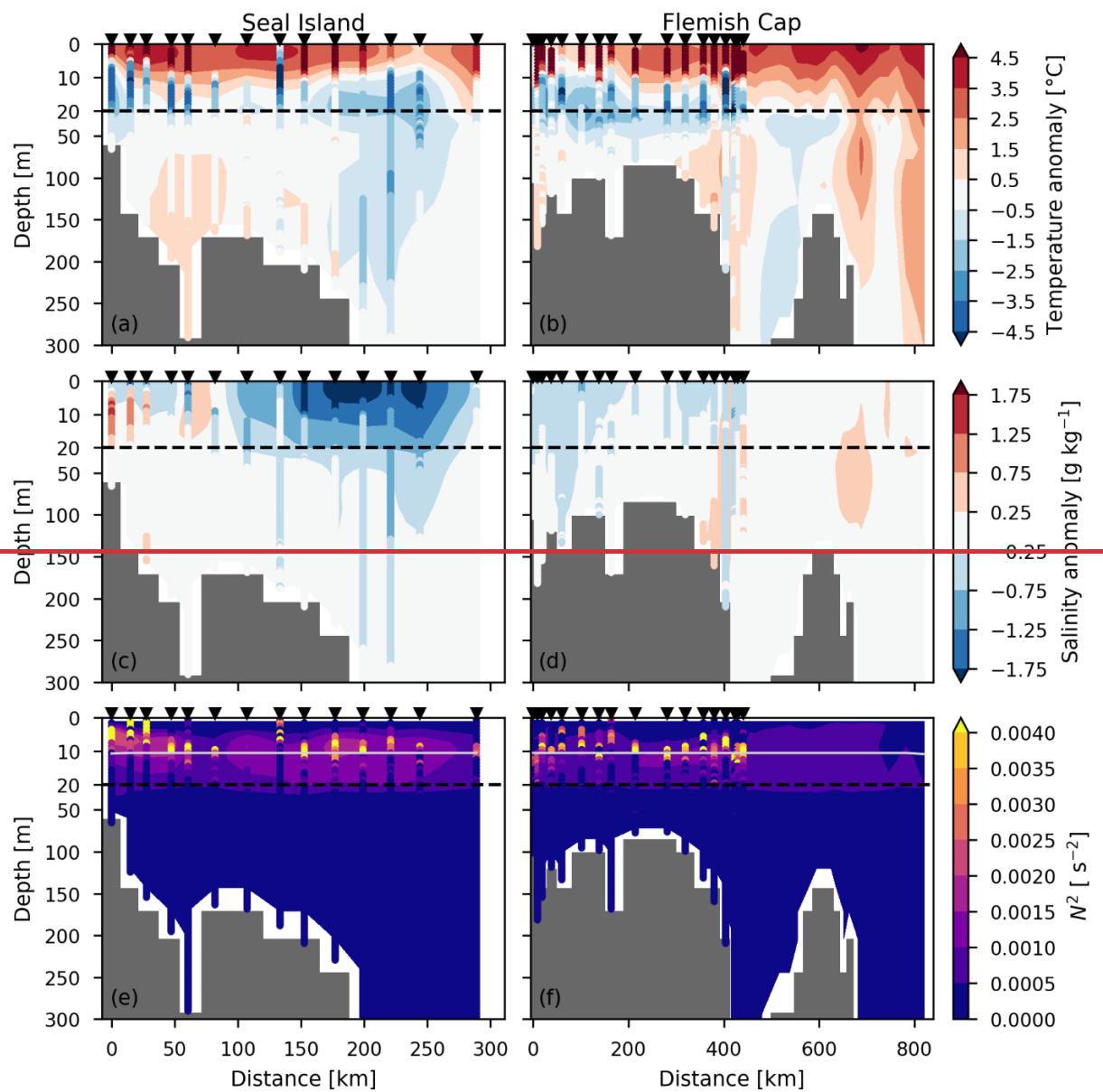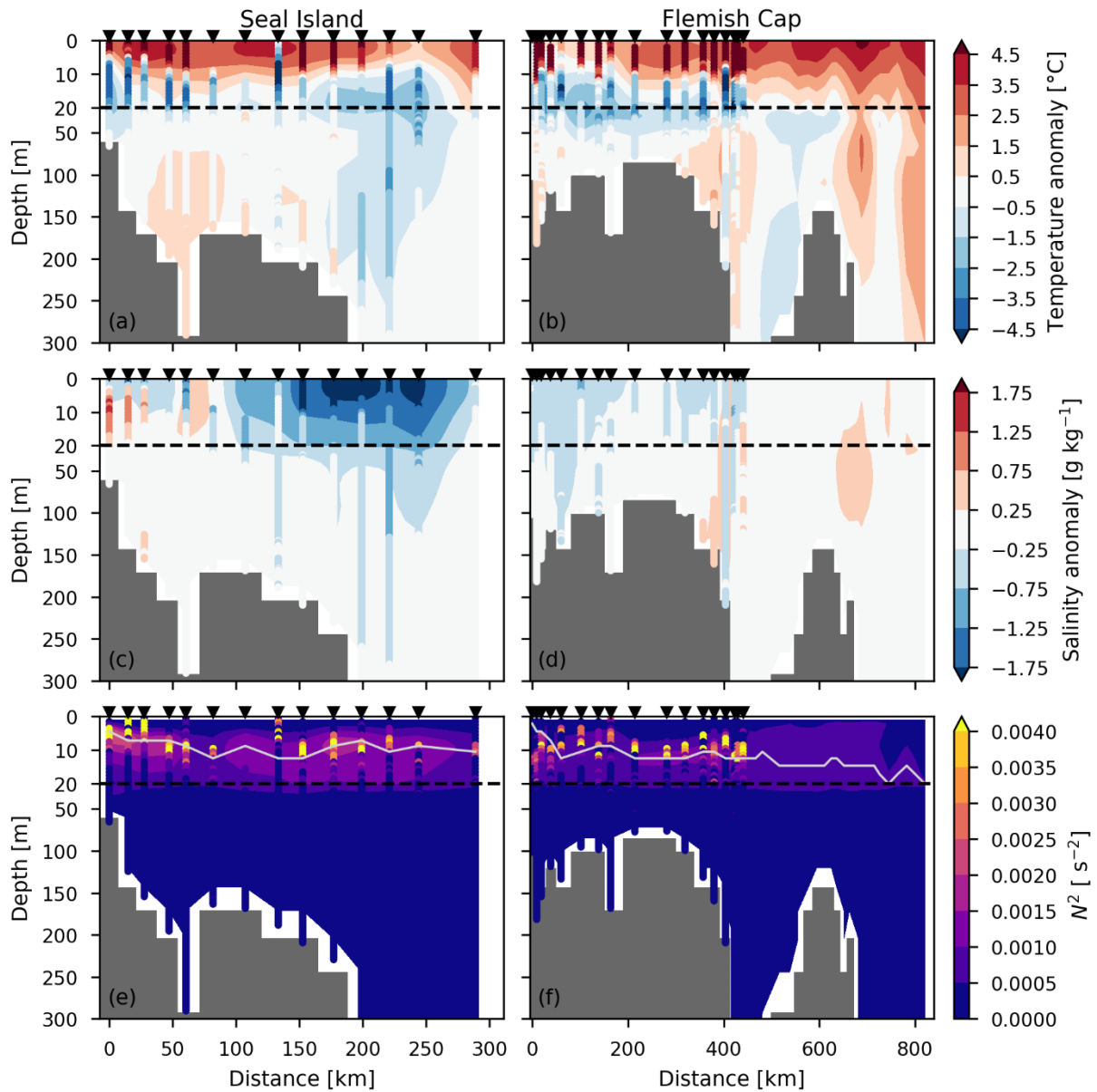
Figure 3: Vertical cross section of temperature anomalies (top), salinity anomalies (middle), and squared-buoyancy frequency (bottom) along the Seal Island (left) and Flemish Cap (right) transects shown for AZMP July 2023 occupation dates. For Seal Island, the AZMP occupation occurred on July 25. For Flemish Cap, the stations inshore of 200 km were sampled on July 20 and the others were sampled on July 30. GLORYS12V1 data (product ref. no. 1) matched to the AZMP sampling dates are shown in shaded contours, and AZMP data (product ref. no. 2) are shown in the coloured circles which appear as lines extending from top to bottom. In the bottom panels, the solid gray line represents the ~~GLORYS12V1~~ mixed layer depth _defined as the depth of the maximum squared-buoyancy frequency_. For Flemish Cap, GLORSY12V1 data at locations offshore of approximately 400 km, which were not sampled by AZMP in July 2023, are taken as the mean of July 20 and July 30. A reference period of 1993-2022 is used to calculate climatologies for both GLORYS12V1 and AZMP. For AZMP, all July and August occupations in the reference period were used to construct the climatology. The black triangles represent the positions of the AZMP stations sampled in July 2023. Note the difference in vertical scale above and below 20 m (black dashed line).

224

225   The anomaly structures of vertical profiles for both temperature and salinity suggest high stratification during the AZMP

226   occupations in July. The squared-buoyancy frequency and mixed layer depth during those occupations, shown in Fig. 3 (e)

227   and (f), indicate stratified conditions in the upper 20 m of the water column. Furthermore, high stratification was apparent at

228   Station 27 in both the GLORYS12V1 and AZMP data throughout nearly the entire summer and early fall (Fig. 4 (b)). High

229   stratification is partially explained by the anomalously cold spring which resulted in a colder than typical subsurface layer and,

230   in turn, strong vertical temperature gradients when surface warming commenced as a result of solar heating (see Fig. S6, S7).

231   Furthermore, the 0-20 m freshwater density in Fig. 4 (d) reveals fresher than typical near-surface conditions from July through

232   October. This fresh anomaly was concentrated in the upper 20 m (see Fig. S5), further explaining the higher than usual

233   stratification. The source of the fresh anomaly is not yet clear but it is present in both the GLORYS12V1 and observations

234   (Fig. 3 (c) and (d)). Fresh water input due to sea ice melt from both local and remote areas is a possible explanation.

235   Unfortunately sea ice in GLORYS12V1 may not be helpful to describe this as its sea ice cover doesn't appear to match

236   observations very well, with no sea ice present in July 2023 or even in the 90th percentile of the 1993-2022 climatology (Fig.

237   4 (e)).

238

239   Another factor that impacts stratification is the degree of vertical mixing introduced by wind forcing at the ocean surface. The

240   10-metre wind speeds from ERA5 (product ref. no. 3) at Station 27 shown in Fig. 4 (f) demonstrate that periods of below

241   average wind speeds in the summer and fall (e.g., early July, mid-August to early September, and late September to early

242   October) preceded the three heat wave periods identified in Fig. 4. Furthermore, a return to average wind speeds preceded the

243   end of each heat wave period with the exception of a wind event in mid-July. This mid-July event corresponded with a reduction

244   in the Station 27 stratification and was followed by a slight dip in the spatially averaged SST as the cold subsurface layer was

245   mixed with the warm surface. Although the periods of average wind speeds were linked with a pause in heat wave conditions,

246   it is likely that these wind events were not strong enough to significantly erode the strongly stratified conditions introduced by

247   a cold spring and fresh early summer. In turn, cold subsurface conditions (from about 20-50 m; not shown), high stratification,

248   and retention of heat near the surface persisted throughout most of the summer and fall.

249

250   Additionally, heat transfer between the ocean and atmosphere is an important element to consider (see Fig. 4 (g) and (h), and

251   Fig. S2). During the July MHW, the 2-metre air temperature from ERA5 was extremely high: at times, it was greater than the

252   annual maximum of the climatological 90th percentile (Fig. 4 (h)). Furthermore, the net surface heat flux was anomalously

253   high during the first few days of the July MHW event but approached anomalously low values as the event reached its end.

254   Similarly, the September and October MHWs exhibited higher than average air temperature and surface heat flux, although

255   not every period in 2023 with these conditions resulted in a MHW (e.g., mid to late January, mid-May, December).

256

257

258
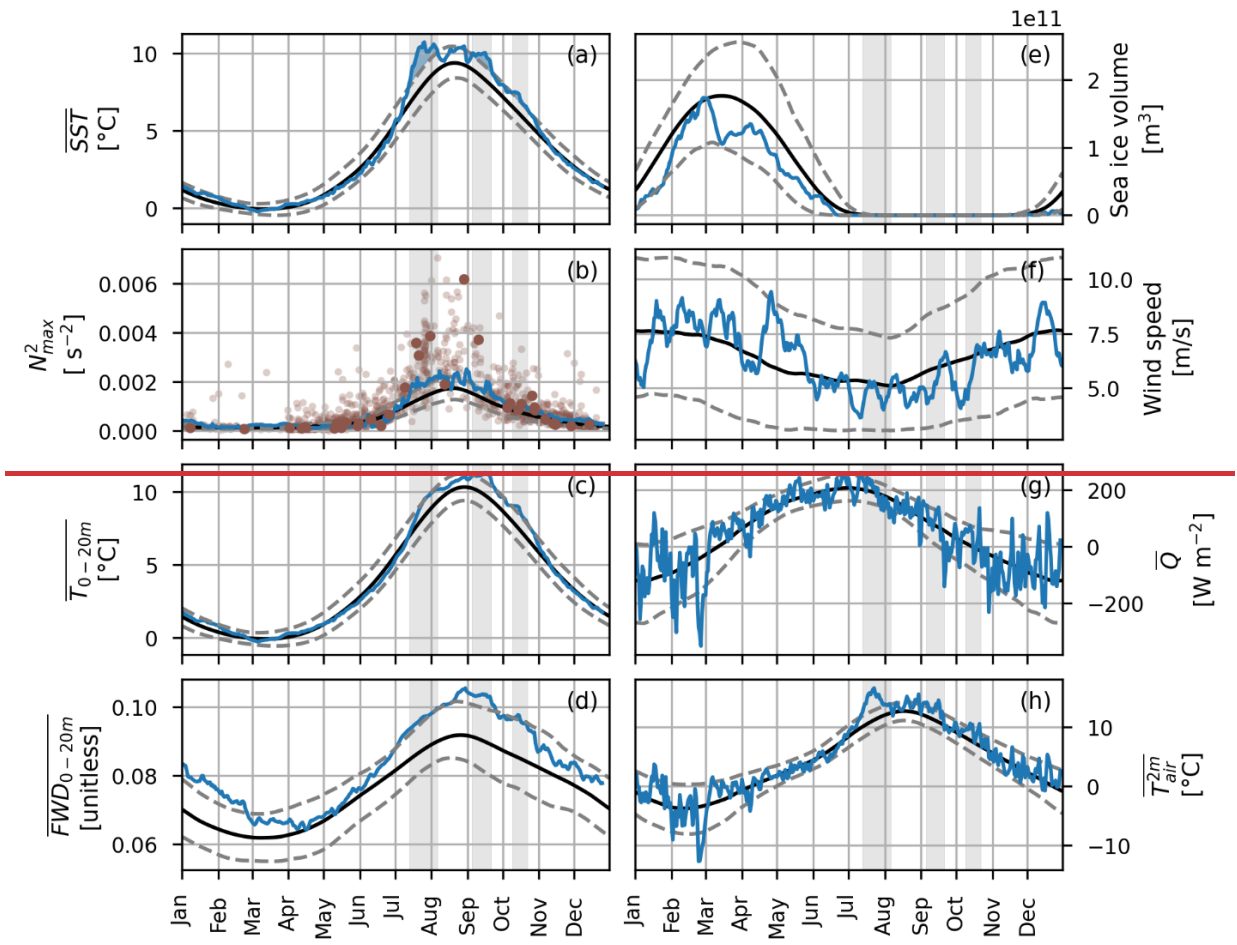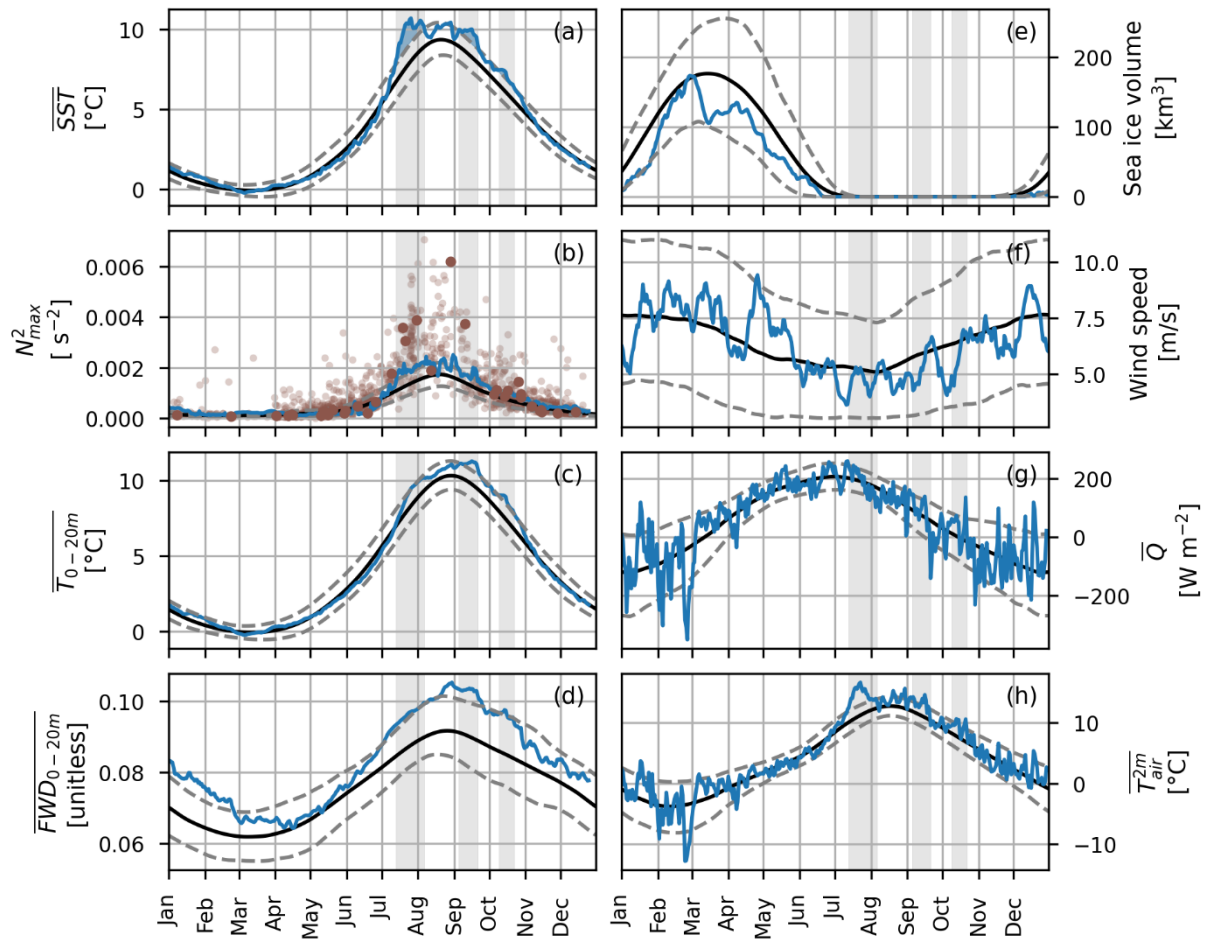
259 **Figure 4: Time series plots for 2023 in blue, the 1993-2022 climatology in black, and the 1993-2022 10th and 90th percentiles in grey**
260 **dashed lines. Variables from GLORYS12V1 (product ref. no. 1) are (a) sea surface temperature averaged over the NL Shelf, (b)**
261 **maximum squared-buoyancy frequency at Station 27, (c) depth-averaged temperature from 0-~~20m~~20 m averaged over the NL Shelf,**
262 **(d) freshwater density from 0-~~20m~~20 m averaged over the NL Shelf, and e) sea ice volume over the NL Shelf. ERA5 (product ref.**
263 **no. 3) variables include (f) 10-metre wind speed at Station 27, (g) net daily-average, surface heat flux averaged over the NL Shelf**
264 **(where positive indicates a downward flux), and (h) 2-metre air temperature averaged over the NL Shelf. Maximum squared-**
265 **buoyancy frequency data at Station 27 from AZMP (product ref. no. 2) are shown in b) for 2023 in large dark brown dots and for**
266 **1993-2022 in small light brown dots. Heat wave periods are indicated by the grey shading.**

267

268 Finally, the role of advection is illustrated by examining the evolution of surface temperature and freshwater density anomalies

269 as well as the vertical maximum of the squared-buoyancy frequency along the shelf (Fig. 5). First, advection is evident where

270 periods of positive freshwater density anomaly and high stratification that are seen in May through June in the upstream parts

271 of the transects (approximately 0 km to 200 km) gradually propagate downstream. These anomalously fresh conditions arrived

272 at Seal Island by the time of the mid-July MHW, increasing the stratification to above typical conditions (see Fig. S4 for

273 climatological stratification). Throughout the shelf, there is typically a link between periods of increased freshwater density

274 and increased stratification (see Fig. S3 and S4), suggesting advected and/or local fresh water input plays an important role in
275 establishing stratification in this region. Advection may also impact sea surface temperatures through the transport of warm
276 water masses. However, during the July MHW, advection of warm anomalies is not apparent in Fig. 5. Rather, this event was
277 nearly simultaneous and wide-spread across the entire shelf. Advection of warm water may have been a contributor for the
278 September through October MHW downstream of Seal Island, although, a more detailed analysis is warranted in the future.

279
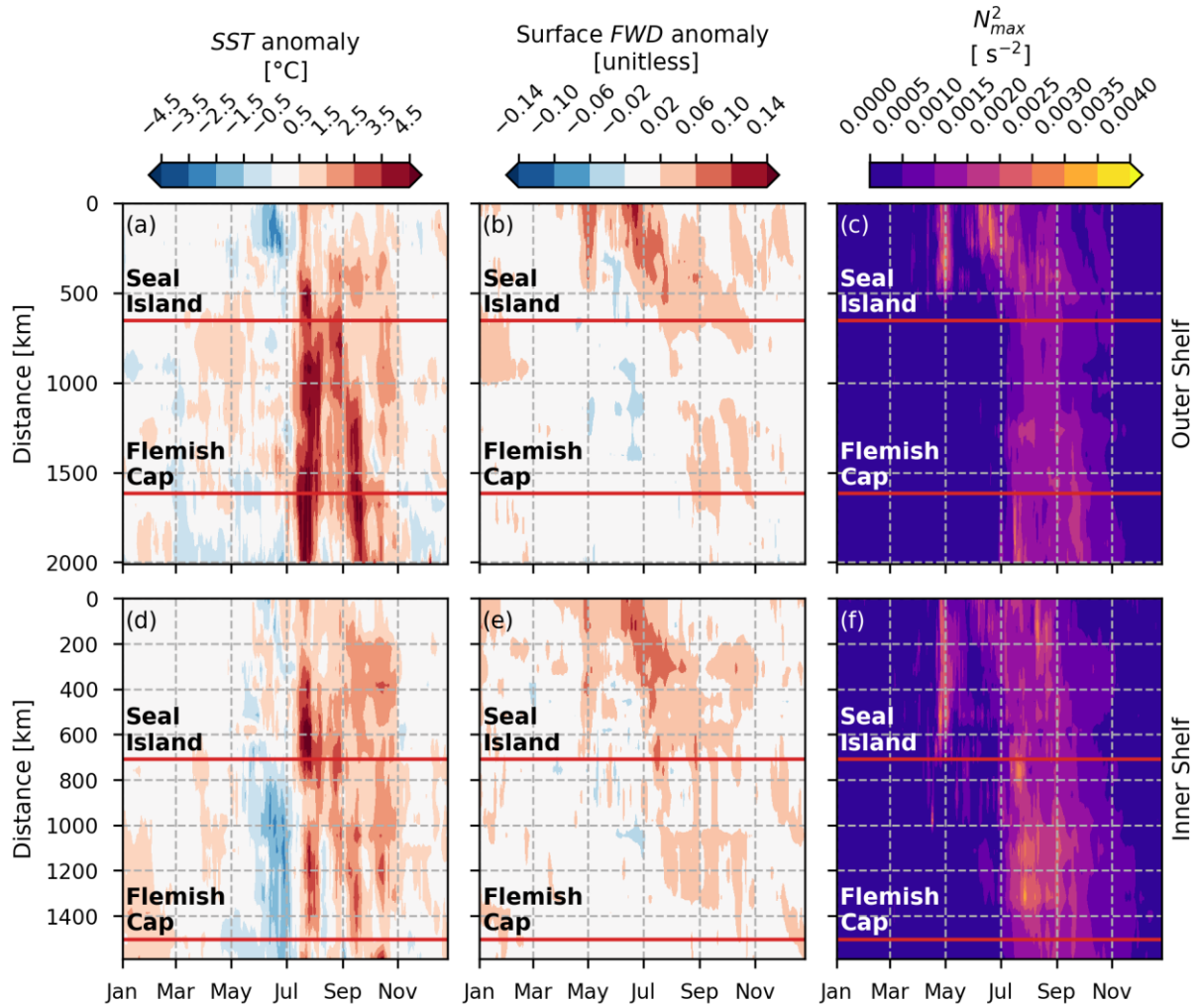
280
281 **Figure 5: Time series of GLORYS12V1 (product ref. no 1) sea surface temperature anomaly (left), surface freshwater density**
282 **anomaly (middle), and vertical maximum of the squared-buoyancy frequency (right) along the Outer Shelf (top) and Inner Shelf**
283 **(bottom) transects for year 2023. See Fig. 1 (a) for Outer Shelf and Inner Shelf transect definitions. Distance is measured along each**
284 **transect starting from the most upstream station. The red horizontal lines represent the along-shelf locations of the Seal Island**
285 **(upper) and Flemish Cap (lower) transects. A reference period of 1993-2022 is used to calculate the climatology used to determine**
286 **the anomalies.**

287

4 Discussion and conclusions

A combination of factors illustrated in Fig. 6 resulted in the series of MHWs detected on the NL Shelf in 2023. As an example, stratification increased as the surface layer warmed in July, preconditioned by unusually cold water temperatures in the spring. In addition, conditions were fresher than typical in the upper 20 m (e.g. Fig. 3 (c), Fig. 4 (d), Fig. 5 (b) and (e), Fig. S5 (c)-(d)). Although the source of these fresh conditions was not analysed in this work, other studies suggest that increased Arctic sea ice melt and freshwater release from the Beaufort Gyre are responsible for recent freshening trends in the North Atlantic (Wang et al., 2024; Yashayaev, 2024). In other regions, Barkhordarian et al. (2024) and Richaud et al. (2024) link abrupt sea ice melt and strong stratification with intensified surface MHWs in the Arctic. In 2023, sea ice conditions on the Labrador Shelf were above normal in June leading to late last occurrence on the southern Labrador Shelf and decreased very rapidly to zero prior to mid-July (Cyr et al., 2024c, Galbraith et al., 2024). Additionally, periods of low winds during the summer maintained the high stratification by limiting vertical mixing. As a result, heat was retained near the surface resulting in a series of MHWs throughout the summer and fall. This series was interrupted by occasional wind events which excited vertical mixing and reduced SSTs. Recent work by Sun et al. (2024) indicate a strong correlation between changes in the oceanic mixed layer depth and the occurrence of MHWs globally, highlighting an important connection between mixed layer restratification and surface MHWs.
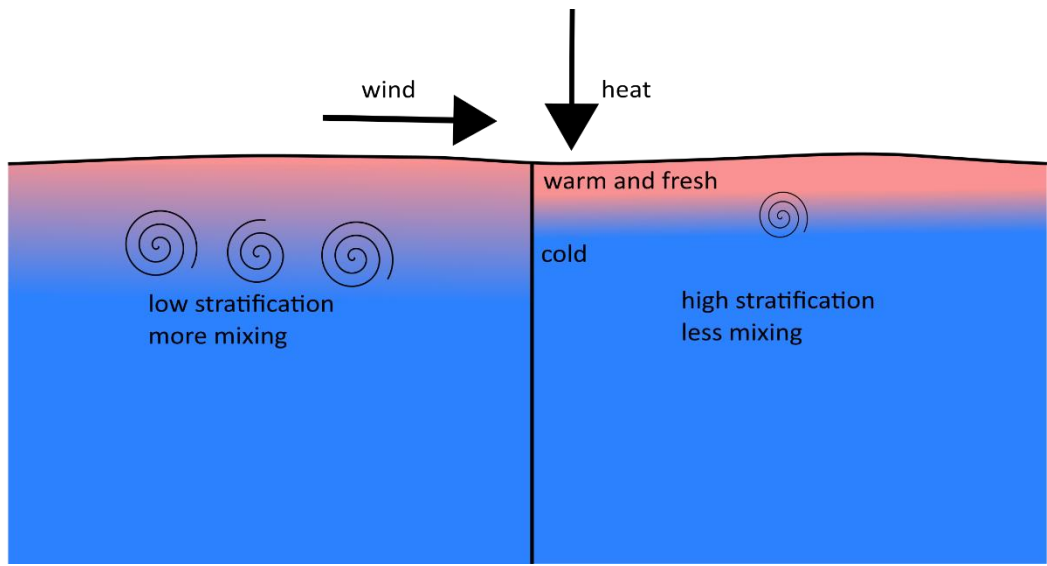
Figure 6: Schematic diagram describing the role of increased stratification on surface MHWs. On the left, lower stratification leads to more mixing. On the right, higher stratification leads to less mixing. Both scenarios receive the same heat flux and wind forcing at the surface. The case with higher stratification results in higher SSTs because the heat is confined to the surface due to less mixing.

The role of air-sea interactions and heat transfer between the atmosphere and the ocean are also important. During the July MHW, the 2-metre air temperature was extremely high, exceeding the annual maximum of the 1993-2022 climatological 90th

percentile for nearly half of the duration of the event. The 2-metre air temperature was also higher than normal during the other MHWs in 2023. Previous work by Schlegel et al. (2021) indicates that latent heat flux is an important driver during the onset of MHWs. Indeed, during the beginning of each MHW on the NL Shelf in 2023, the net surface heat flux was higher than typical (Fig. 4 (g)) driven by positive anomalies in the surface latent heat flux and the surface long-wave radiation (Fig. S2). Yet, not all periods of anomalously positive net surface heat flux resulted in a MHW, suggesting a combination of oceanic and atmospheric processes were at play in these surface MHWs.

The role of advection should also be considered. The Labrador Current is responsible for transporting water properties southward along the NL Shelf. For example, the anomalously fresh conditions detected at Seal Island in July (Fig. 3 (c)) were transported south carrying with them properties such as high stratification. Indeed, Fig. 2 (d)-(f) and Fig. 5 (a)-(b) show signs that warm anomalies were potentially associated with transport from NNS in August to the outer (inner) edges of GB (FC) in September. A bifurcation of the Labrador Current exists near the northern boundary of GB, directing some of the conditions associated with warm anomalies along the coast of GB in October. However, the October onset of MHWs in LS and NNS and the abrupt initiation of the July MHW across the entire shelf cannot be explained by transport. These events are more likely linked with local meteorological and oceanographic conditions.

A more thorough investigation quantifying the magnitude of these factors and relationships with large-scale atmospheric conditions is considered for future work in the NL Shelf region. For instance, a heat budget analysis in the mixed layer (see Oliver et al., 2021 as an example) could quantify the role of various elements such as air-sea interaction, transport, vertical mixing, etc., in establishing MHW conditions. Furthermore, processes such as mesoscale eddies (e.g., Sun et al., 2024) and changes in coastal and shelf-break upwelling (e.g., Reyes-Mendoza et al., 2022) are likely to influence surface temperatures in the NL Shelf region. Higher resolution modelling experiments could also be used to explore and quantify controls on MHW conditions, particularly when examining shelf-scale processes that are not resolved by or well-constrained by global reanalysis products.

Finally, impacts of MHWs on the NL Shelf ecosystem is an important area for future work. One area of interest is the vertical distribution of MHWs (e.g., Fig. S5) because not all elements of the marine ecosystem are impacted by high sea surface temperatures. Furthermore, regional differences in MHW intensity, frequency, and duration are important elements when considering ecosystem impacts. Tools such as ocean model reanalyses, analyses, and forecasts can aid in near real-time monitoring by linking surface MHWs with vertical characteristics such as stratification and by exploring spatial structures in remote areas that are difficult to study directly with observations. These results suggest that ocean model nowcast and reanalysis products can complement observational methods for studying MHWs in near-real time over large geographic areas and at multiple depths.

Data and code availability

The data used in this study are available as described in Table 1. The code used in this study can be accessed via a GitLab repository upon request via email to the corresponding author.

Author contribution

NS conducted the analysis, produced the visualisations, and prepared the initial manuscript draft. NS, HJA, and JC organised and curated data. All authors contributed to conceptualization of the study, discussions on methodology and results, and editing and reviewing the manuscript.

Competing interests

The authors declare that they have no conflict of interest.

Acknowledgements

We thank two anonymous reviewers for constructive comments on the manuscript. Hersbach et al. (2023) was downloaded from the Copernicus Climate Change Service (2023). The results for ERA5 contain modified Copernicus Climate Change Service information 1993-2023. Neither the European Commission nor ECMWF is responsible for any use that may be made of the Copernicus information or data it contains. We greatly appreciate input and discussions with David Bélanger regarding 2023 nutrient inventories and primary productivity and thoughtful comments from Pierre Pepin. This work is a contribution to the science mission of the Atlantic Zone Monitoring Program.

References

Barkhordarian, A., Nielsen, D.M., Olonscheck, D., and Baehr, J.: Arctic marine heatwaves forced by greenhouse gases and triggered by abrupt sea-ice melt, Commun. Earth Environ., 5, 57, https://doi.org/10.1038/s43247-024-01215-y, 2024.

Copernicus Climate Change Service: ERA5 hourly data on single levels from 1940 to present. Copernicus Climate Change Service (C3S) Climate Data Store (CDS), DOI: 10.24381/cds.adbb2d47, last access: 04 April 2024, 2023.

Copernicus: https://climate.copernicus.eu/global-sea-surface-temperature-reaches-record-high, last access: 08 May 2024, 2023.

Coyne, J., Cyr, F., Donnet, S., Galbraith, P., Geoffroy, M., Hebert, D., Layton, C., Ratsimandresy, A., Snook, S., Soontiens, N., and Walkusz, W.: Canadian Atlantic Shelf Temperature-Salinity (CASTS). Federated Research Data Repository [dataset], https://doi.org/10.20383/102.0739, 2023.

Cyr, F. and Galbraith, P. S.: A climate index for the Newfoundland and Labrador shelf, Earth Syst. Sci. Data, 13, 1807–1828, https://doi.org/10.5194/essd-13-1807-2021, 2021.

Cyr, F., Lewis, K., Bélanger, D., Regular, P., Clay, S., and Devred, E.: Physical controls and ecological implications of the timing of the spring phytoplankton bloom on the Newfoundland and Labrador shelf, Limnol. Oceanogr. Lett. https://doi.org/10.1002/lol2.10347, 2024a.

Cyr, F., Adamack, A., Bélanger, D., Koen-Alonso, M., Mullowney, D., Murphy, H., Regular, P., and Pepin, P.: Environmental Control on the Productivity of a Heavily Fished Ecosystem, Research Square [preprint], https://doi.org/10.21203/rs.3.rs-4108948/v1, 27 March 2024b.

Cyr, F., Coyne, J., Snook, S., Bishop, C., Galbraith, P.S., Chen, N., Han, G.: Physical Oceanographic Conditions on the Newfoundland and Labrador Shelf during 2023, Can. Tech. Rep. Hydrogr. Ocean Sci. 382: iv + 54 p., 2024c.

Denaxa, D., Korres, G., Bonino, G., Masina, S., and Hatzaki, M.: The role of air–sea heat flux for marine heatwaves in the Mediterranean Sea, in: 8th edition of the Copernicus Ocean State Report (OSR8), edited by: von Schuckmann, K., Moreira, L., Grégoire, M., Marcos, M., Staneva, J., Brasseur, P., Garric, G., Lionello, P., Karstensen, J., and Neukermans, G., Copernicus Publications, State Planet, 4-osr8, 11, https://doi.org/10.5194/sp-4-osr8-11-2024, 2024.

Drévillon, M., Fernandez, E., Lellouche, J.M.: EU Copernicus Marine Service Product User Manual for the Global Ocean Physics Reanalysis, GLOBAL_MULTIYEAR_PHY_001_030, Issue 1.5, Mercator Ocean International, https://catalogue.marine.copernicus.eu/documents/PUM/CMEMS-GLO-PUM-001-030.pdf, last access: 19 March 2024, 2023

Drévillon, M., Lellouche, J.M., Régnier, C., Garric, G., Bricaud, C., Hernandez, O., and Bourdallé-Badie, R.: EU Copernicus Marine Service Quality Information Document for the Global Ocean Physics Reanalysis, GLOBAL_MULTIYEAR_PHY_001_030, Issue 1.6, Mercator Ocean International, https://catalogue.marine.copernicus.eu/documents/QUID/CMEMS-GLO-QUID-001-030.pdf, last access: 19 March 2024, 2023

402 Edwing, K., Wu, Z., Lu, W., Li, X., Cai, W.-J., and Yan, X.-H.: Impact of Marine Heatwaves on Air-Sea CO2 Flux Along the
403 US East Coast, Geophy. Res. Lett., 51, e2023GL105363, https://doi.org/10.1029/2023GL105363, 2024.

405 EU Copernicus Marine Service Product: Global Ocean Physics Reanalysis, Mercator Ocean International [dataset],
406 https://doi.org/10.48670/moi-00021, 2023.

408 Fratantoni, P. S., and Pickart, R. S.: The western North Atlantic shelfbreak current system in summer, J. Phys. Oceanogr.,
409 37(10), 2509-2533, https://doi.org/10.1175/JPO3123.1, 2007.

411 Frölicher, T.L., Laufkötter, C.: Emerging risks from marine heat waves, Nat. Commun., 9, 650,
412 https://doi.org/10.1038/s41467-018-03163-6, 2018.

414 Galbraith, P. S., Blais, M., Lizotte, M., Cyr, F., Bélanger, D., Casault, B., Clay, S., Layton, C., Starr, M., Chassé, J., Azetsu-
415 Scott, K., Coyne, J., Devred, E., Gabriel, C.-E., Johnson, C. L., Maillet, G., Pepin, P., Plourde, S., Ringuette, M. Shaw, J.-L.,
416 Oceanographic conditions in the Atlantic zone in 2023, Can. Tech. Rep. Hydro. and Ocean Sci., 379 : v + 39 p., 2024.

418 Geoffroy, M., Bouchard, C, Flores, H., Robert, D., Gjøsæter, H., Hoover, C., Hop, H., Hussey, N. E., Nahrgang, J., Steiner,
419 N., Bender, M., Berge, J., Castellani, G., Chernova, N., Copeman, L., David, C. L., Deary, A., Divoky, G., Dolgov, A. V.,
420 Duffy-Anderson, J., Dupont, N., Durant, J. M., Elliott, K., Gauthier, S., Goldstein, E. D., Gradinger, R., Hedges, K., Herbig,
421 J., Laurel, B., Loseto, L., Maes, S., Mark, F. C., Mosbech, A., Pedro, S., Pettitt-Wade, H., Prokopchuk, I., Renaud, P. E.,
422 Schembri, S., Vestfals, C., and Walkusz, W.: The circumpolar impacts of climate change and anthropogenic stressors on Arctic
423 cod (Boreogadus saida) and its ecosystem, Elem. Sci. Anth., 11, 1, https://doi.org/10.1525/elementa.2022.00097, 2023.

425 Han, G., Ma Z., and Chen, N.: Ocean climate variability off Newfoundland and Labrador over 1979–2010: A modelling
426 approach, Ocean Modelling,144, 101505, https://doi.org/10.1016/j.ocemod.2019.101505, 2019.

428 Hersbach H., Bell B., Berrisford P., Hirahara, S., Horányi, A., Muñoz-Sabater, J., Nicolas, J., Peubey, C., Radu, R., Schepers,
429 D., Simmons, A., Soci, C., Abdalla, S., Abellan, X., Balsamo, G., Bechtold, P., Biavati, G., Bidlot, J., Bonavita, M., De Chiara,
430 G., Dahlgren, P., Dee, D., Diamantakis, M., Dragani, R., Flemming, J., Forbes, R., Fuentes, M., Geer, A., Haimberger, L.,
431 Healy, S., Hogan, R. J., Hólm, E., Janisková, M., Keeley, S., Laloyaux, P., Lopez, P., Lupu, C., Radnoti, G., de Rosnay, P.,
432 Rozum, I., Vamborg, F., Villaume, S., and Thépaut, J.-N.: The ERA5 global reanalysis. Q. J. R. Meteorol. Soc., 146, 1999–
433 2049. https://doi.org/10.1002/qj.3803, 2020.

435   Hersbach, H., Bell, B., Berrisford, P., Biavati, G., Horányi, A., Muñoz Sabater, J., Nicolas, J., Peubey, C., Radu, R., Rozum,

436   I., Schepers, D., Simmons, A., Soci, C., Dee, D., Thépaut, J-N: ERA5 hourly data on single levels from 1940 to present.

437   Copernicus Climate Change Service (C3S) Climate Data Store (CDS), DOI: 10.24381/cds.adbb2d47, last access: 05 April

438   2024, 2023.

440   Hobday, A. J., Alexander, L. V., Perkins, S. E., Smale, D. A., Straub, S. C., Oliver, E. C. J., Benthuysen, J. A., Burrows, M.

441   T., Donat, M. G., Feng, M., Holbrook, N. J., Moore, P. J., Scannell, H. A., Sen Gupta, A., and Wernberg, T.: A hierarchical

442   approach to defining marine heatwaves, Prog. Oceanogr. 141, 227-238, https://doi.org/10.1016/j.pocean.2015.12.014, 2016.

444   Hobday, A. J., Oliver, E. C. J., Sen Gupta, A., Benthuysen, J. A., Burrows, M. T., Donat, M. G., Holbrook, N. J.,. Moore, P.

445   J., Thomsen, M. S., Wernberg, T., Smale, D. A.: Categorizing and naming marine heatwaves, Oceanography, 31(2), 162–173,

446   https://doi.org/10.5670/oceanog.2018.205, 2018.

448   IPCC: IPCC Special Report on the Ocean and Cryosphere in a Changing Climate [H.-O. Pörtner, D.C. Roberts, V. Masson-

449   Delmotte, P. Zhai, M. Tignor, E. Poloczanska, K. Mintenbeck, A. Alegría, M. Nicolai, A. Okem, J. Petzold, B. Rama, N.M.

450   Weyer (eds.)].   Cambridge   University   Press,   Cambridge,   UK   and   New   York,   NY,   USA,   755   pp.

451   https://doi.org/10.1017/9781009157964, 2019

453   IPCC: Climate Change 2023: Synthesis Report. Contribution of Working Groups I, II and III to the Sixth Assessment Report

454   of the Intergovernmental Panel on Climate Change [Core Writing Team, H. Lee and J. Romero (eds.)]. IPCC, Geneva,

455   Switzerland, pp. 35-115, doi: 10.59327/IPCC/AR6-9789291691647, 2023.

457   Jutras, M., Dufour, C.O., Mucci, A., and Talbot, L.C. : Large-scale control of the retroflection of the Labrador Current, Nat.

458   Commun., 14, 2623, https://doi.org/10.1038/s41467-023-38321-y, 2023.

460   Lazier, J. R. N., and Wright, D. G.: Annual velocity variations in the Labrador Current, J. Phys. Oceanogr., 23(4), 659-678,

461   https://doi.org/10.1175/1520-0485(1993)023<0659:AVVITL>2.0.CO;2, 1993.

463   Le Grix, N., Zscheischler, J., Laufkötter, C., Rousseaux, C. S., and Frölicher, T. L.: Compound high-temperature and low-

464   chlorophyll extremes in the ocean over the satellite period, Biogeosciences, 18, 2119–2137, https://doi.org/10.5194/bg-18-

465   2119-2021, 2021.

467   Lellouche, J.-M., Grenier, E., Bourdallé-Badie, R., Garric, G., Melet, A., Drévillon, M., Bricaud, C., Hamon, M., Le Galloudec,

468   O., Regnier, C., Candela, T., Testut, C.-E., Gasparin, R., Ruggiero, G., Benkiran, M., Drillet, R., and Le Traon, P.-Y.: The

469 Copernicus Global 1/12° Oceanic and Sea Ice GLORYS12 Reanalysis, Front. Earth Sci., 9, 698876,
470 https://doi.org/10.3389/feart.2021.698876, 2021.

472 McAdam, R., Masina, S., and Gualdi, S.: Seasonal forecasting of subsurface marine heatwaves, Commun. Earth Environ., 4,
473 225, https://doi.org/10.1038/s43247-023-00892-5, 2023.

475 McDougall, T. J. and Barker, P. M.: Getting started with TEOS-10 and the Gibbs Seawater (GSW) Oceanographic Toolbox,
476 28 pp., SCOR/IAPSO WG127, ISBN 978-0-646-55621-5, 2011.

478 McDougall, T. J., Barker, P. M., Holmes, R. M., Pawlowicz, R., Griffies, S. M., and Durack, P. J.: The interpretation of
479 temperature and salinity variables in numerical ocean model output and the calculation of heat fluxes and heat content, Geosci.
480 Model Dev., 14(10), 6445-6466, https://doi.org/10.5194/gmd-14-6445-2021, 2021.

482 NOAA National Centers for Environmental Information: ETOPO 2022 15 Arc-Second Global Relief Model, NOAA National
483 Centers for Environmental Information, https://doi.org/10.25921/fd45-gt74, last access: 17 December 2024, 2022.

485 Oliver, E. C. J., Donat, M. G., Burrows, M.T., Moore, P. J., Smale, D. A., Alexander, L. V., Benthuysen, J. A., Feng, M., Sen
486 Gupta, A., Hobday, A. J., Holbrook, N. J., Perkins-Kirkpatrick, S. E., Scannell, H. A., Straub, S. C., and Wernberg, T.: Longer
487 and more frequent marine heatwaves over the past century, Nat. Commun., 9, 1324, https://doi.org/10.1038/s41467-018-
488 03732-9, 2018.

490 Oliver, E. C. J., Benthuysen, J. A., Darmaraki, S., Donat, M. G., Hobday, A. J., Holbrook, N. J., Schlegel, R. W., and Sen
491 Gupta, A.: Marine heatwaves, Annu. Rev. Mar. Sci., 13, 313-342, https://doi.org/10.1146/annurev-marine-032720-095144,
492 2021.

494 Open Government, Ecosystem Production Units in the Northwest Atlantic, Government of Canada:
495 https://open.canada.ca/data/en/dataset/9a515ef8-0e2a-479e-9b25-55658eae30be, last access: 15 February 2024, 2014.

497 Pepin, P., Higdon, J., Koen-Alonso, M., Fogarty, M., and Ollerhead, N.: Application of ecoregion analysis to the identification
498 of Ecosystem Production Units (EPUs) in the NAFO Convention Area, NAFO Sci. Counc. Res. Doc, 14/069, 2014.

500 Perez, E., Ryan, S., Andres, M., Gawarkiewicz, G., Ummenhofer, C. C., Bane, J., and Haines, S.: Understanding physical
501 drivers of the 2015/16 marine heatwaves in the Northwest Atlantic, Sci. Rep., 11, 17623, https://doi.org/10.1038/s41598-021-
502 97012-0, 2021.

503

504 Petrie, B: Does the north Atlantic oscillation affect hydrographic properties on the Canadian Atlantic continental shelf?
505 Atmosphere-Ocean, 45(3), 141–151, https://doi.org/10.3137/ao.450302, 2007.

506

507 Poitevin P., Thébault J., Siebert V., Donnet S., Archambault P., Doré J., Chauvaud L., and Lazure P.: Growth Response of
508 Arctica Islandica to North Atlantic Oceanographic Conditions Since 1850, Front. Mar. Sci. 6:483, doi:
509 10.3389/fmars.2019.00483, 2019.

510

511 Reyes−Mendoza, O., Manta, G., and Carrillo, L.: Marine heatwaves and marine cold-spells on the Yucatan Shelf-break
512 upwelling region, Continental Shelf Research, Volume 239, 104707, https://doi.org/10.1016/j.csr.2022.104707, 2022.

513

514 Richaud, B., Hu, X., Darmaraki, S., Fennel, K., Lu, Y., and Oliver, E. C. J.: Drivers of marine heatwaves in the Arctic Ocean,
515 J. Geophy. Res-Oceans, 129(2), e2023JC020324, https://doi.org/10.1029/2023JC020324, 2024

516

517 Schlegel, R.W., Oliver, E. C. J. and Chen, K.: Drivers of Marine Heatwaves in the Northwest Atlantic: The Role of Air–Sea
518 Interaction During Onset and Decline, Front. Mar. Sci., 8, 627970, https://doi.org/10.3389/fmars.2021.627970, 2021.

519

520 Sims, L. D., Subrahmanyam, B., and Trott, C. B.: Ocean–Atmosphere Variability in the Northwest Atlantic Ocean during
521 Active Marine Heatwave Years, Remote Sensing, 14(12), 2913, https://doi.org/10.3390/rs14122913, 2022.

522

523 Smith, K. E., Burrows, M. T., Hobday, A. J., G. King, N. G., Moore, P. J., Sen Gupta, Thomsen, M., S., Wernberg, T., and
524 Smale, D. A.: Biological impacts of marine heatwaves, Annu. Rev. Mar. Sci., 15, 119-145, https://doi.org/10.1146/annurev-
525 marine-032122-121437, 2023.

526

527 Sun, W., Wang, Y., Yang, Y., Yang, J., Ji, J., and Dong, C.: Marine heatwaves/cold-spells associated with mixed layer depth
528 variation globally. Geophy. Res. Lett., 51(24), e2024GL112325, https://doi.org/10.1029/2024GL112325, 2024.

529

530 Templeman, N.D.: Ecosystem Status and Trends Report for the Newfoundland and Labrador Shelf. DFO Can. Sci. Advis. Sec.
531 Res. Doc. 2010/026 vi + 72 pp., 2010.

532

533 Therriault, J.-C., Petrie, B., Pepin, P., Gagnon, J., Gregory, D., Helbig, J., Herman, A., Lefaivre, D., Mitchel, M., Pelchat, B.,
534 Runge, J., and Sameoto, D.: Proposal for a Northwest Atlantic Zonal Monitoring Program, Can. Tech. Rep. Hydro. and Ocean
535 Sci., 194, vii + 57 pp., 1998.

536

537 Urrego-Blanco, J., and Sheng, J.: Interannual Variability of the Circulation over the Eastern Canadian Shelf. Atmosphere-
538 Ocean, 50(3), 277–300. https://doi.org/10.1080/07055900.2012.680430, 2012.

539

540 Wang, Q., Danilov, S., and Jung, T: Arctic freshwater anomaly transiting to the North Atlantic delayed within a buffer zone.
541 Nat. Geosci. 17, 1218–1221, https://doi.org/10.1038/s41561-024-01592-1, 2024.

542

543 World Meteorological Organization: WMO guidelines on the calculation of climate normals, Tech. rep., Geneva, Switzerland,
544 2017.

545

546 Wu, Y., Peterson, I. K., Tang, C. C. L., Platt, T., Sathyendranath, S., and Fuentes-Yaco, C.: The impact of sea ice on the
547 initiation of the spring bloom on the Newfoundland and Labrador Shelves, J. Plankton Res., 29(6), 509–514,
548 https://doi.org/10.1093/plankt/fbm035, 2007.

549

550 Yashayaev, I.: Intensification and shutdown of deep convection in the Labrador Sea were caused by changes in atmospheric
551 and freshwater dynamics. Commun Earth Environ 5, 156, https://doi.org/10.1038/s43247-024-01296-9, 2024.